Fibre Diffraction Review 13, 31 - 37, 2005 doi: 10.1382/fdr.2005.1301

The Interpretation of Simultaneous Small and Wide-angle X-ray Scattering Data Collected During Quiescent Cnrystallisation

S. Hanna

H.H. Wills Physics Laboratory, University of Bristol, Tyndall Avenue, Bristol, BS8 1TL

Abstract

Small and wide-angle X-ray scattering patterns have been calculated from randomly oriented stacks of lamellar crystals of isotactic polypropylene, at various stages during a hypothetical growth process. When the crystals have a small lateral width, it is possible to detect a long-period peak in the small-angle pattern when the crystalline wide-angle trace is too weak to be detected above the background noise. This finding has important implications for the interpretation of simultaneous small and wide-angle X-ray data collected during quiescent crystallization experiments. In particular, it challenges the suggestion that such measurements provide evidence for crystal growth through spinodal decomposition.

Keywords: *SAXS; WAXS; Polymer Crystallisation; Spinodal Decomposition.*

Introduction

Recently there has been considerable interest in studying the development of crystallinity in semi-crystalline polymers, using simultaneous measurements of small and wide-angle X-ray scattering (SAXS and WAXS) patterns. The value of such measurements lies in the fact that it is possible to relate changes in the local arrangements of chains within crystalline lamellae, to developments in the organisation of the lamellae within spherulites or other large scale structures. Performing the measurements simultaneously removes any ambiguity over the nucleation time of the crystallites being studied, allowing a straightforward comparison between the two sets of scattering data.

Simultaneous small and wide-angle measurements are now routine at a number of synchrotron X-ray sources around the world, and several studies of polymer crystallisation have been published [1-14]. A number of authors have noted that, during isothermal crystallisation of certain polymers from the melt, the small-angle patterns appear to develop peaks before there is any sign of crystalline scattering in the wide-angle region [10-13]. This observation has been interpreted by some as meaning that there are density fluctuations in the melt, prior to the formation of crystals. This, in turn, has been used as the basis for a new model of polymer crystalisation, based on the phenomenon of spinodal decomposition [12,15]. In the spinodal model, molten material is said to separate into regions with differing conformational disorder, and hence different densities. The denser regions, i.e. those with more conformational order, are then viewed as the places where crystal nucleation is most likely to occur.

The main aim of the present paper is to examine the experimental basis upon which the spinodal model was built. For this reason, the data of Terrill et al. (see Figure 2 of ref. [11]), which relate to the isothermal crystallisation of isotactic polypropylene (iPP), have been re-examined. It will be shown that, for stacks of crystals with small lateral width, it is possible to observe small-angle scattering, when the wide-angle scattering is below the threshold for observation. Thus the evidence for a spinodal model is far from secure.

Method

The lamellar stack model

The model chosen consists of a stack of growing crystalline lamellae of iPP (see Figure 1). It is assumed that the stack exists, *a priori*, on the grounds that such structures are found at the cores of spherulites of iPP and many other polymers, and thus occur at the earliest stages of crystallisation. No attempt is made to explain the origin of the lamellar stack. It is assumed that the lamellae all increase in width at the same linear rate, and that, at any point in time, all crystallites have the same dimensions. These assumptions may be regarded as highly idealised. However, they have been made in order to minimise the number of parameters in the model. The lamellar thickness, parallel to the chain axis, is assumed constant. Thus, the crystals only grow laterally. In addition, it is assumed

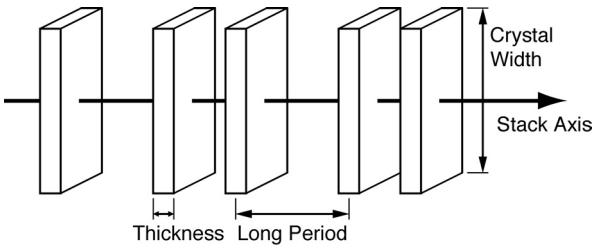

Figure 1: Schematic representation of the lamellar stack used as the basis of the diffraction calculations presented here. The lamellae have an approximately square cross section, and are of uniform thickness parallel to the stack axis. The widths of the lamellae are also uniform, and increase simultaneously and at the same rate.

that the lamellae are approximately square in cross-section perpendicular to the axis of the stack, and that there is no crystallographic register between the crystallites. The positions of the crystalline lamellae are represented by a 1-dimensional paracrystal, with nearest neighbour distribution governed by Gaussian statistics [16,17]. The merits of more sophisticated distribution functions have been discussed elsewhere [18,19].

The crystals are represented as parallelepipeds, with sides parallel to the unit cell axes **a**, **b** and **c**, and dimensions $L_a = N_a a$, $L_b = N_b b$ *and* $L_c = N_c C$. N_a, N_b *and* N_c are the numbers of unit cells parallel to **a**, **b** and **c** respectively, and must be integers for the following analysis to apply. The unit cell parameters for iPP were taken from ref. [20] to be a = 6.65 Å; b = 20.96 Å; c = 6.50 Å; $\alpha = \gamma = 90°$ and $\beta = 99.33°$. In the results presented below, N_c was taken to be 20 unit cells, and the ratio of $N_a = 3N_b$ was maintained so that $L_a \approx L_b$. N_b was varied between 1 and 20 unit cells, corresponding to a variation in crystal width between *ca*. 20Å and ca. 400Å.

The scattered X-ray intensities were calculated from first principles and normalised by the number of lamellae in the stack, in order to ensure that the calculated values were directly comparable between small and wide-angle regions. However, the intensity units quoted are not absolute, because no account was taken of the number of lamellar stacks per unit volume. Further, in order to ensure comparability with experiment, additional geometric correction factors were applied.

Wide-angle scattering calculation

The wide angle scattering from a single lamella was obtained by explicitly summing the scattered amplitudes from all of the unit cells in the crystal [21]. The resulting expression was multiplied by its complex conjugate and averaged over all polarisations of the incident radiation to give:

$$I_{Lamella}(\mathbf{s}) = I_e F(\mathbf{s}) F^*(\mathbf{s}) \frac{\sin^2(\pi N_a \mathbf{s.a})}{\sin^2(\pi \mathbf{s.a})} \cdot \frac{\sin^2(\pi N_b \mathbf{s.b})}{\sin^2(\pi \mathbf{s.b})} \cdot \frac{\sin^2(\pi N_c \mathbf{s.c})}{\sin^2(\pi \mathbf{s.c})} \exp(-Bs^2/2) \qquad (1)$$

where **s** is the scattering vector, related to the scattering angle by $s = (2/\lambda)\sin\theta$, and I_e is the classical scattering from a single electron, which decays as the inverse square of the distance from the sample to the detector. This relationship is of importance when comparing the intensities measured by the small and wide-angle detectors, which are normally at quite different distances. ***F(s)*** is the structure factor for a particular scattering vector, calculated from atomic coordinates for iPP, assuming the *C c* space group [20]. The exponential factor in equation (1) is a temperature factor which accounts for thermal motion. At room temperature, an appropriate value for B is 8.5 Å^2 [20]. However, at 145°C, which is the temperature of the study being considered, B may be modified to 11.9 Å^2, using a harmonic approximation. The overall reduction in intensity as a result of this increase in temperature is around 6% for the main Bragg reflections.

In order to simulate unoriented or powder diffraction data, the diffracted intensity was integrated over all possible orientations, giving, for a stack of N independent lamellae:

$$I_{WAXS}(\mathbf{s}) = \frac{N}{4\pi} \int_0^{2\pi} d\Psi \int_0^{\pi} \sin\Theta d\Theta . I_{Lamella}(\mathbf{s}) L_{WAXS} \qquad (2)$$

The integration in equation (2) was carried out numerically. It should be noted that the intensity given by equation (2) represents the X-ray flux per unit area of the diffraction circle, and implicitly includes the same Lorentz factor that occurs in a powder diffractometer experiment, thus allowing a direct comparison with the experimental data without further correction. The extra factor, L_{WAXS}, takes into account the geometry and sensitivity of the detector, and will be discussed in more detail below.

The amorphous contribution to the wide-angle scattering was not calculated. Instead, the experimental amorphous background was fitted approximately using an analytical function, which was then added to the intensities shown in the results section. No account was taken of crystalline defects in calculating the wide-angle scattering patterns. Since lattice disorder would be expected to broaden and weaken the crystalline reflections, the results presented here should be considered to provide an upper bound on the expected wide-angle peak intensities.

Small-angle scattering calculation

The form factor of a single lamella is given by:

$$I_{Form}(\mathbf{s}) = I_e (n_e V \Delta\rho)^2 \frac{\sin^2(\pi N_a \mathbf{s.a})}{(\pi N_a \mathbf{s.a})^2} \cdot \frac{\sin^2(\pi N_b \mathbf{s.b})}{(\pi N_b \mathbf{s.b})^2} \cdot \frac{\sin^2(\pi N_c \mathbf{s.c})}{(\pi N_c \mathbf{s.c})^2} \qquad (3)$$

where V is the volume of a crystal, n_e is the number of electrons per unit volume of the crystal and $\Delta\rho$ is the fractional difference in density between the crystal and the amorphous matrix. At 145°C, which is the temperature of interest here, the literature value of $\Delta\rho$ is *ca*. 0.15 [22].

The lamellar stack was modelled using a 1-dimensional paracrystal to represent the positions of the centres of mass of the crystals. A Gaussian distance distribution function was employed, with a mean crystal separation $\bar{z} = 200$Å and standard deviations σ = 10, 20 and 40Å. Results were compared from both infinite and finite stacks. For an infinite stack, with N lamellae per unit length, the scattering is given by [16,17]:

$$I_{Stack}(\mathbf{s}) = N I_{Form}(\mathbf{s}) . \Re\left(\frac{1 + H(Z)}{1 - H(Z)}\right) \qquad (4)$$

where $H(Z)$ is the Fourier transform of the nearest neighbour distribution function, and Z is the component of s taken along the stack axis, which is taken to coincide with

the crystallographic *c* axis. For a finite stack of *N* lamellae, the scattered intensity may be written as:

$$I_{Stack}(\mathbf{s}) = NI_{Form}(\mathbf{s}).P(Z) \qquad (5)$$

in which *P(Z)* is given by:

$$P(Z) = 1 + 2\sum_{j=1}^{N-1}\frac{(N-j)}{N}\exp\left[-2j(\pi\sigma Z)^2\right]\cos(2\pi jZ\bar{z}) \qquad (6)$$

As for the wide-angle calculation, the diffracted small-angle intensity was integrated over all possible orientations, to give:

$$I_{SAXS}(\mathbf{s}) = \frac{1}{4\pi}\int_0^{2\pi} d\Psi \int_0^{\pi} \sin\Theta d\Theta . I_{Stack}(\mathbf{s}) L_{SAXS}(2\theta) \qquad (7)$$

L_{SAXS} is a machine dependant correction factor, and the integration in equation (7) was performed numerically.

Machine dependent correction factors

Before it is possible to compare the calculated traces for the small and wide-angle regions of the diffraction patterns, it is necessary to correct for the detector geometry employed. The data of ref. [11] were collected at the simultaneous SAXS/WAXS facility at Daresbury. The wide-angle data were collected using a curved Inel 1-dimensional position sensitive detector, 0.3m from the sample, and the small-angle data collection used a quadrant detector at a distance of 3.5m. The resolutions of the two detectors are nominally 0.1° for the Inel detector and 250 μm for the quadrant detector. It is assumed that the resolutions can be used to define the active areas of each channel of the detectors. The correction factors consist of the product of the active area in each case, with an attenuation factor:

$$\begin{aligned} L_{WAXS} &= \left(0.1^\circ \times \frac{\pi}{180^\circ}\right) \times lr \times A_W \\ L_{SAXS} &= (250\mu m) \times \frac{2\pi r \sin 2\theta}{4} \times A_S \end{aligned} \qquad (8)$$

in which *l* is the aperture of the Inel detector perpendicular to the knife-edge, and AW and AS are the relevant attenuation factors, required to avoid saturating the detectors. Typical values for these parameters are *l* = 5mm [23] and AW =0.4 AS [24]. *r* is the sample-detector distance relevant to each detector. It is also assumed that the quantum efficiencies of the two detectors are the same.

Results

Figure 2 shows SAXS and WAXS patterns calculated for infinite stacks of iPP lamellae at 145°C, for nominal crystal widths ranging between 20 and 400Å, using $\bar{z}$ = 200Å and σ = 20Å. The crystal widths indicated on the graphs are nominal, since the actual widths must be an integral number of unit cells. The most striking feature observed is that the small-angle peak, at *s* ~ 0.005Å^{-1} is much more intense than the main Bragg reflections in the wide-angle trace. In fact, for this particular model, the small-angle peak is *ca*.5 times more intense than the wide angle-peaks, for a given crystal width. This result can be seen more clearly in *Figure 3*, in which the intensities of the small and wide angle peaks are compared as a function of nominal crystal width.

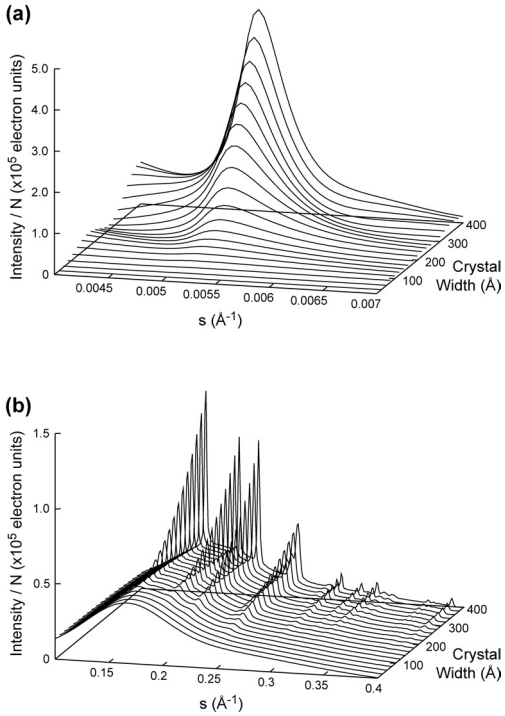

Figure 2: Calculated (a) SAXS and (b) WAXS patterns for infinite stacks of iPP lamellae at 145°C, for nominal crystal widths between 20 and 400Å, using $\bar{z}$ = 200Å and σ = 20Å . The intensities are given as multiples of the scattering expected from a single electron (electron units), and are normalised by the number of lamellae per unit length of the stack, *N*. (s = (2/λ)sin *θ*).

The large disparity in the peak intensities raises the question of whether it is possible for the small-angle peak to be visible when the wide-angle peaks are not. The visibility of the peaks will depend on a combination of the sensitivity of the X-ray detector and the X-ray counting statistics. If it is assumed that the small and wide-angle detectors have the same sensitivity, it is clear from *Figure 3* that the wide-angle peaks will not be visible until some time after the small-angle peak has appeared. For example, if the horizontal dotted line in Figure 3 represents an arbitrary threshold, in this case 4 x 10^3 electron units, above which the peaks may be detected, then it can be seen that the SAXS peak will become visible at a crystal width of ~70Å, while the (110) reflection will not be visible until ~120Å, as indicated by the arrows labelled (1) and (2) respectively.

Poor X-ray counting statistics will also affect the wide-angle traces more than the small-angle ones. This is partly because of the lower absolute intensity of the wide-angle trace, but mainly because the crystalline reflections

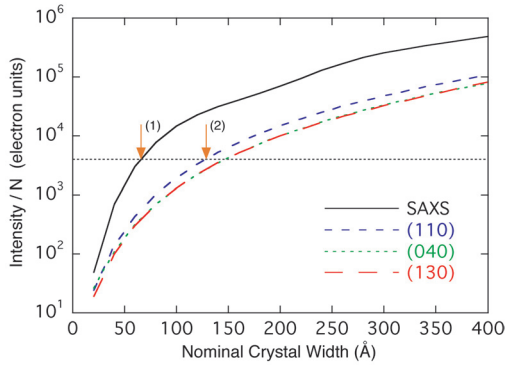

Figure 3: Semi-log plot showing the variation in intensities of the small-angle peak, and the principal wide-angle reflections in Figure 2, with nominal crystal width. The value taken for the small-angle intensity is the maximum value of the small-angle peak. The horizontal dotted line indicates how, for a given detection limit, the small-angle peak will be detected before the Bragg peaks are visible. Arrows (1) and (2) are referred to in the text.

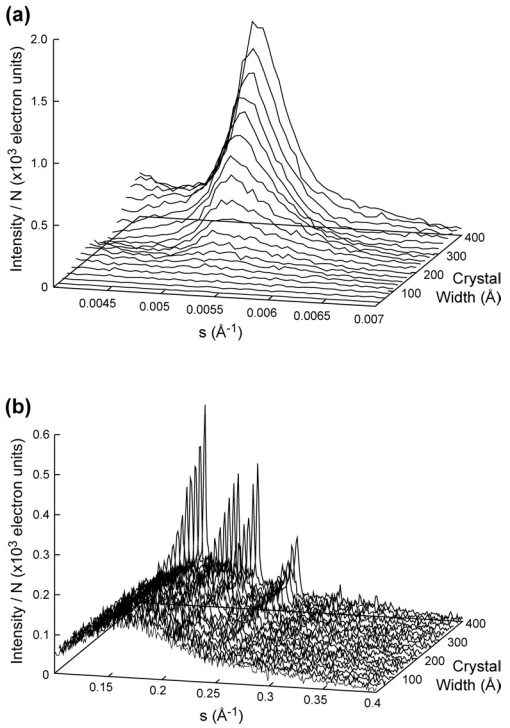

Figure 4: Calculated (a) SAXS and (b) WAXS patterns for the same model as in Figure 2. The intensities have been scaled and Poisson noise has been added, as described in the text ($s = (2/\lambda)\sin\theta$).

are superimposed on a substantial amorphous halo. This means that, when the crystalline reflections are weak i.e. at early crystallisation times, they may be lost in the noise resulting from the amorphous background. This effect is demonstrated in *Figure 4*, where the scattering curves from *Figure 2* have been scaled by a constant amount and random Poisson noise has been added. The amount of scaling was chosen in order to get an approximate match in noise levels between *Figure 4* and the published traces. It is clear from *Figure 4*, that the visibility of the wide-angle peaks is profoundly affected by the amount of background noise present, whereas the small-angle peak, by virtue of its greater intensity and larger signal-to-noise ratio, is still clearly apparent. In the results shown, the small-angle peak is visible from crystal widths of ~100Å, while the wide-angle peaks are not visible until the crystal width reaches ~200Å.

Discussion

Model Predictions

From the results shown in *Figures* 2,3 and 4, it is clear that the simple lamellar stack model presented here is capable of producing qualitatively similar behaviour to that observed experimentally. The main observation, that the SAXS intensity is much greater that the WAXS intensity, leads to the conclusion that, as a consequence of the relative signal-to-noise ratios, there will be situations in which the SAXS peak is observable where the WAXS peaks are not. This conclusion is consistent with the data of Terrill et al. (*Figure* 2 of ref. [11]), which, indeed, shows that the wide-angle traces are noisier, and hence of lower intensity, than the small-angle ones. Thus, it appears that the experimental data *may* be accounted for by a conventional model of stacks of lamellae, and that it is not necessary to invoke a model of spinodal decomposition in order to explain the observations. This point will be discussed further below.

It is, in fact, a common observation in published simultaneous SAXS/WAXS experiments that the wide-angle data are noisier, than the corresponding small-angle data (*e.g.* see refs. [3,11,13,25]). This finding must, in part, be due to the types of detector in use. For example, Hsiao and coworkers [25] have studied the sensitivity of the wide-angle detector on the X27C beamline at Brookhaven National Laboratory, using model alkane systems, and have concluded that the lower limit of detection in this case is 0.56% crystallinity. These workers have also reported data similar to ref. [11] for iPP.

Model Deficiencies

It would be wrong to claim that the lamellar stack model presented here can provide an exact match to the experimental data. The model has several deficiencies, and is certainly not correct in detail. The main criticism of the lamellar stack model must be that it is too ideal. It has been assumed that the crystals have sharp edges, are all the same size and grow at exactly the same rate. In reality, the crystals would be expected to vary both in thickness and in width, and there should be a more diffuse boundary between the crystalline and amorphous phases. These factors would lead to changes in the form of equations (3) and (4) which would affect the small-angle peak height and width. Also, the calculated SAXS profiles are narrower than those of ref. [11], which is a consequence of the choice of interlamellar distance distribution function. More sophisticated models for infinite paracrystalline stacks have been discussed at length by several

other authors [18,19,26-30] and it is clear that there is scope for considerable modification to both the width and the overall shape of the small-angle peak. The most likely outcome of any such refinement to the model would be to broaden the peak and slightly diminish its intensity.

The results shown in *Figures* 2 to 4 were based on the assumption that the stack of crystals was of infinite extent. However, inspection of electron micrographs suggests that a stack of between 5 and 10 lamellae would be more appropriate. The effect of stack size on the small-angle peak intensity is illustrated in *Figure* 5. For a given variation in interlamellar spacing (σ = 20Å) the peak intensity falls by about one third and the width increases by about 50% on reducing the size of the stack to N=5. A smaller change is observed for N=10. The peak shape is also sensitive to variations in σ, and it can be seen, that small decreases in σ can lead to significant increases in the peak height. Thus finite and infinite stack models produce similar predictions for the small-angle peak intensity, with the exact intensity and peak shape being sensitive to the choice of N and σ. Any realistic model should include a distribution of stacks with different values for N, σ and z, as was invoked to explain the SAXS data from polyethylene [31].

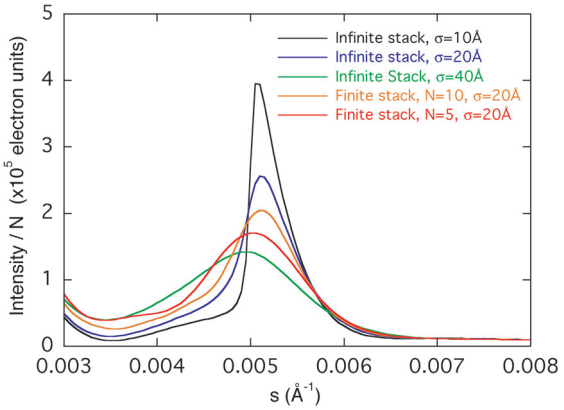

Figure 5: Small-angle peak profiles for several different lamellar stack models. In all cases, the mean interlamellar spacing, z, is 200Å, and the crystal width is nominally 300Å.

Other deficiencies in the model, include the lack of lattice distortions, mosaic structure and other forms of disorder, which would broaden and weaken the wide-angle peaks without affecting the small-angle peaks, and uncertainties over the exact sensitivities and quantum efficiencies of the detectors used experimentally.

Spinodal Analysis

Although the intensities shown in *Figure* 2a were generated on the assumption of a uniformly growing lamellar stack, it is interesting, nevertheless, to analyse them as if they resulted from a Cahn-Hilliard model of spinodal decomposition [32,33]. The Cahn-Hilliard analysis consists, essentially, of looking for a peak in the graph of $R(s)$ versus s, in which R(s) is the growth rate of the logarithm of the scattered intensity:

$$R(s) = \frac{d \log_e I_{Stack}(s,t)}{dt} \qquad (9)$$

It is interesting to consider whether the present model could produce such a maximum.

The discussion will be limited, initially, to the intensity distribution along the crystallographic c^* axis. In this case, we may write, in place of equation (5):

$$I_{Stack}(s,t) = const. \times V^2(t) \times G(s) \qquad (10)$$

where:

$$G(s) = \frac{\sin^2(\pi N_c \mathbf{s.c})}{(\pi N_c \mathbf{s.c})^2}.P(Z) \qquad (11)$$

and $V(t)$ is the time-varying volume of crystals. Taking logarithms, we have:

$$\log_e I_{Stack}(s,t) = const. + 2\log_e V(t) + \log_e G(s) \qquad (12)$$

from which it is clear that the growth rate will be independent of s, irrespective of the crystal growth kinetics. The separation of variables in equation (12) occurs because the form factor, $G(s)$, is independent of time. This is only true along the c^* axis: in other regions of reciprocal space, we have an additional factor due to the crystal width, of:

$$\frac{\sin^2(\pi N_a \mathbf{s.a})}{(\pi N_a \mathbf{s.a})^2} \times \frac{\sin^2(\pi N_b \mathbf{s.b})}{(\pi N_b \mathbf{s.b})^2} \qquad (13)$$

in which N_a and N_b both increase with time. However, the process of orientational averaging leads only to a weak dependence of growth rate on s, as shown in *Figure* 6. In the figure, it is assumed that N_a and N_b increase linearly with time, and $R(s)$ is calculated by performing a least squares fit to the scattered intensities from the earliest part of the growth process (*i.e.* from 20 to 100Å). For a spinodal process we would expect the peak to be considerably more obvious.

It would appear that the only way to obtain a true maximum in $R(s)$ is if the form of the small angle scattering factor, $G(s)$, changes during the initial development of the stack. This could result for example from changes in the thickness, or density, as the lamellae are initially established. Indeed there have been several recent studies which have followed the development of the crystalline morphology in polyethylene from isolated lamellae to well defined stacks [34-37]. However, such refinements would be difficult to include in the current model in anything other than an *ad hoc* manner, and will not be considered further here.

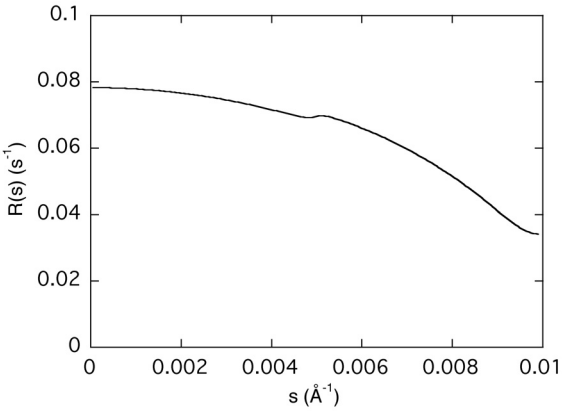

Figure 6: Plot of *R(s) versus s* for an infinite lamellar stack, with z = 200Å and σ = 20Å, with *R(s)* calculated over the interval from crystal widths of 20 to 100Å.

Thus the model, as presented, is able to reproduce the key feature of the experimental data i.e. the presence of a small-angle peak in the absence of wide-angle peaks, but cannot explain the experimental growth kinetics without further development.

Conclusions

X-ray scattering calculations have been performed, based on a simple model of a stack of growing crystalline lamellae of iPP. The model indicates that it is possible to observe the main interlamellar peak in the small-angle scattering pattern at early times in the crystal growth, when the wide-angle crystalline reflections are too weak to be observed over the background noise. The model can therefore explain the lack of crystalline reflections in experimental data from quiescent crystallisation studies of iPP, without the need to invoke spinodal decomposition. However, the uniformly growing lamellar stack model, as presented here, is too simplistic to reproduce the early-stage growth kinetics reported by Ryan and coworkers [10-12]. A more complete model would need to consider the initial stages of the development of order in growing crystals in more detail.

Acknowledgements

This paper was based on an oral contribution delivered at the 12th Annual CCP13 Fibre Diffraction and Non-Crystalline Diffraction Workshop in Cambridge, July 2003. The author would like to thank Dr. Peter Barham for initially suggesting the analysis described in this paper, and for providing electron micrographs and crystallisation data from isotactic polypropylene. He would also like to thank Drs. W. Bras, J.K. Hobbs, P.D. Olmsted and N.J. Terrill, and Profs. D.J. Blundell, J.S. Higgins and A.J. Ryan for several stimulating discussions during the preparation of this paper.

References

[1] Laggner, P. and Mio, H. Nucl. Instrum. Meth. Phys. Res. (1992), A323, 86-90.

[2] Bras, W., Derbyshire, G.E., Ryan, A.J., Mant, G.R., Felton, A., Lewis, R.A., Hall, C.J. and Greaves, G.N. Nuc. Inst. Meth. Phys. Res. (1993), A326, 587-591.

[3] Zachmann, H.G. and Wutz, C. in Crystallisation of Polymers M. Dosière Ed., NATO ASI-C series on Mathematical and Physical Sciences, Vol. 405, (Kluwer, Dordrecht, Netherlands) (1993), pp.559-564.

[4] Ryan, A.J., Naylor, S., Komanschek, B., Bras, W., Mant, G.R. and Derbyshire, G.E. ACS Symposium Series, (1994), 581, 162-180.

[5] Haswell, R., Van Mechelen, J.B., Mensch, C.T.J. and De Groot, H. Nucl. Instrum. Meth. Phys. Res. (1995), B97, 242-247.

[6] Ezquerra, T.A., López-Cabarcos, E., Hsiao, B.S. and Baltà-Calleja, F.J. Phys. Rev. E, (1996), 54, 989-992.

[7] Hamley, I.W., Fairclough, J.P.A., Ryan, A.J., Bates, F.S. and Towns-Andrews, E. Polymer, (1996), 37, 4425-4429.

[8] Fougnies, C., Damman, P., Villers, D., Dosiere, M. and Koch, M.H.J. Macromolecules, (1997), 30, 1385-1391.

[9] Rueda, D.R., Gutierrez, M.C.G., Ania, F., Zolotukhin, M.G. and Baltà-Calleja, F.J. Macromolecules, (1998), 31, 8201-8208.

[10] Ryan, A.J., Terrill, N.J. and Fairclough, J.P.A. ACS PMSE Prep. (1998), 79, 358-359.

[11] Terrill, N.J., Fairclough, P.A., Towns-Andrews, E., Komanschek, B.U., Young, R.J. and Ryan, A.J. Polymer (1998), 39, 2381-2385.

[12] Ryan, A.J., Fairclough, J.P.A., Terrill, N.J., Olmsted, P.D. and Poon, W.C.K. Faraday Discuss. (1999), 112, 13-29.

[13] Hsiao, B.S., Wang, Z., Yeh, F., Gao. Y. and Sheth, K.C. Polymer (1999), 40, 3515-3523.

[14] Lefebvre, X., Koch, M.H.J., Reynaers, H. and David, C. J. Polym. Sci. B - Polym. Phys., (1999), 37, 1-18.

[15] Olmsted, P.D., Poon, W.C.K., McLeish, T.C.B., Terrill, N.J. and Ryan, A.J. Phys. Rev. Lett., (1998), 81, 373.

[16] Vonk, C.G. in Small Angle X-ray Scattering, O. Glatter, & O. Kratky Eds. (Academic Press, London) (1982), pp433-466.

[17] Hosemann, R. and Bagchi, S.N. Direct Analysis of Diffraction by Matter (North Holland, Amsterdam) (1962), pp408-420.

[18] Crist, B. J. Polym. Sci.: Polym. Phys. Ed. (1973), 11, 635-661.

[19] Crist, B. and Morosoff, N. J. Polym. Sci.: Polym. Phys. Ed. (1973), 11, 1023-1045.

[20] Natta, G. and Corradini, P. Nuovo Cimento Suppl. (1960), 15, 40.

[21] Warren, B.E. X-ray Diffraction (Addison-Wesley, Massachusetts) (1969), pp27-30.
[22] Albrecht, T. and Strobl, G. Macromolecules (1995), 28, 5267-5273.
[23] Bras, W. Private communication (1999).
[24] Terrill, N.J. Private communication (1999).
[25] Wang, Z., Hsiao, B.S., Kopp, C., Sirota, E.B., Agarwal, P. and Srinivas, S. ACS PMSE Prep. (1999), 81, 355-356.
[26] Hall, I.H. and Toy, M. in Structure of Crystalline Polymers edited by I.H. Hall (Elsevier Applied Science Publishers, London) (1984), pp181-228.
[27] Blundell, D.J. Acta Cryst. (1970), A26, 472-476.
[28] Blundell, D.J. Acta Cryst. (1970), A26, 476-483.
[29] Ruland, W. Colloid and Polym. Sci. (1977), 255, 417-427.
[30] Blundell, D.J. Polymer (1978), 19, 1258-1266.
[31] Strobl, G. and Müller, N. J. Polym. Sci.: Polym. Phys. Ed. (1973), 11, 1219-1233.
[32] Cahn, J.W. and Hilliard, J.E. J. Chem. Phys. (1958), 28, 258.
[33] Cahn, J.W. J. Chem. Phys. (1965), 42, 93-99.
[34] Tashiro, K., Sasaki, S. and Kobayashi, M. Macromolecules (1996), 29, 7460.
[35] Tashiro, K., Sasaki, S. and Kobayashi, M. Polym. J. (1998), 30, 485.
[36] Sasaki, S., Tashiro, K., Kobayashi, M., Izumi, Y. and Kobayashi, K. Polymer (1999), 40, 7125-7135.
[37] Akpalu, Y.A. and Amis, E.J. J. Chem. Phys. (1999), 111, 8686-8695.